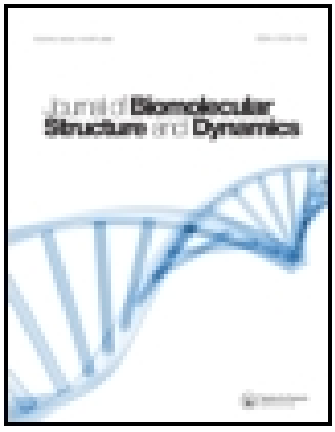

Journal of Biomolecular Structure and Dynamics
Publication details, including instructions for authors and subscription information:
http://www.tandfonline.com/loi/tbsd20

Energy-optimised pharmacophore approach to identify potential hotspots during inhibition of Class II HDAC isoforms

Shabir Ahmad Ganai[a], Karthi Shanmugam[b] & Vijayalakshmi Mahadevan[ab]

[a] Centre for Nanotechnology & Advanced Biomaterials (CeNTAB), School of Chemical & Biotechnology, SASTRA University, Thanjavur 613401, India

[b] Department of Bioinformatics, School of Chemical & Biotechnology, SASTRA University, Thanjavur 613401, India

Published online: 27 Jan 2014.

To cite this article: Shabir Ahmad Ganai, Karthi Shanmugam & Vijayalakshmi Mahadevan (2014): Energy-optimised pharmacophore approach to identify potential hotspots during inhibition of Class II HDAC isoforms, Journal of Biomolecular Structure and Dynamics, DOI: 10.1080/07391102.2013.879073

To link to this article: http://dx.doi.org/10.1080/07391102.2013.879073

Journal of Biomolecular Structure and Dynamics, 2014
http://dx.doi.org/10.1080/07391102.2013.879073

Energy-optimised pharmacophore approach to identify potential hotspots during inhibition of Class II HDAC isoforms

Shabir Ahmad Ganai[a], Karthi Shanmugam[b] and Vijayalakshmi Mahadevan[a,b]*

[a]*Centre for Nanotechnology & Advanced Biomaterials (CeNTAB), School of Chemical & Biotechnology, SASTRA University, Thanjavur 613401, India;* [b]*Department of Bioinformatics, School of Chemical & Biotechnology, SASTRA University, Thanjavur 613401, India*

Communicated by Ramaswamy H. Sarma

(*Received 26 September 2013; accepted 22 December 2013*)

Histone deacetylases (HDACs) are conjugated enzymes that modulate chromatin architecture by deacetylating lysine residues on the histone tails leading to transcriptional repression. Pharmacological interventions of these enzymes with small molecule inhibitors called Histone deacetylase inhibitors (HDACi) have shown enhanced acetylation of the genome and are hence emerging as potential targets at the clinic. Type-specific inhibition of Class II HDACs has shown enhanced therapeutic benefits against developmental and neurodegenerative disorders. However, the structural identity of class-specific isoforms limits the potential of their inhibitors in precise targeting of their enzymes. Diverse strategies have been implemented to recognise the features in HDAC enzymes which may help in identifying isoform specificity factors. This work attempts a computational approach that combines *in silico* docking and energy-optimised pharmacophore (E-pharmacophore) mapping of 18 known HDAC inhibitors and has identified structural variations that regulate their interactions against the six Class II HDAC enzymes considered for the study. This combined approach establishes that inhibitors possessing higher number of aromatic rings in different structural regions might function as potent inhibitors, while inhibitors with scarce ring structures might point to compromised potency. This would aid the rationale for chemical optimisation and design of isoform selective HDAC inhibitors with enhanced affinity and therapeutic efficiency.

Keywords: histone deacetylases; histone deacetylase inhibitor; molecular docking; molecular mechanics-generalised born surface area; energy-optimised pharmacophore

1. Introduction

Transcriptional regulation in eukaryotic cells is predominantly anchored through chromatin (Li, Carey, & Workman, 2007). Modulation of chromatin states through acetylation and deacetylation of histone proteins has evolved as a key mechanism in disease and development in eukaryotes (Kouzarides, 2007). Histone deacetylases (HDACs) and histone acetyl transferases (HATs) are conjugated enzymes that exert antagonistic function and have demonstrated success in clinical trials as effective anticancer agents (Kuo & Allis, 1998; Kurdistani & Grunstein, 2003; Tan, Cang, Ma, Petrillo, & Liu, 2010).

HDACs fall into the group of zinc-containing metalloenzymes that deacetylate the histone proteins, leading to chromatin condensation. NAD^+-dependent enzymes (sirtuins) are a group of HDACs investigated extensively for clinical applications (Witt, Deubzer, Milde, & Oehme, 2009). The functional balance between HATs and HDACs is a crucial factor in gene expression programs and cell cycle progression events. Aberrant recruitment of HDACs has been shown to be linked to neurodegenerative diseases, leukemias and muscular dystrophy (Colussi et al., 2008; Rivieccio et al., 2009; Van Damme et al., 2012). Overexpression of HDAC6 has been reported in oral squamous cell carcinoma (Sakuma et al., 2006), during neurodegeneration events (Rivieccio et al., 2009) and in the epithelial to mesenchymal transition of lung carcinoma cells during metastasis (Shan et al., 2008). Active functional roles of HDAC4 have been shown to confer radioresistance to cancer cells by augmenting DNA damage repair and have been implicated in breast cancer (Geng et al., 2006). Upregulation of HDAC5 and HDAC7 are linked to transition events in colorectal cancer (Watamoto et al., 2003).

The 18 HDACs identified so far in mammals fall into four structurally and phylogenetically distinct classes. While Class I and Class II HDACs are zinc-dependent amidohydrolases, the Class III HDACs called sirtuins are NAD^+-dependent enzymes (de Ruijter, Gennip, Caron, Kemp, & Kuilenburg, 2003; Gregoretti, Lee, & Goodson, 2004; Witt et al., 2009). Literature has extensively documented the localisation

*Corresponding author. Email: mviji@sastra.edu

of Class I and Class IV HDACs predominantly in the nucleus. Class II HDACs are tissue specific and some of these shuttles from the cytoplasm to the nucleus and vice versa. HDACs thus have distinct functions in cell proliferation, cellular differentiation and development (Fischle, Kiermer, Dequiedt, & Verdin, 2001). The diverse functional roles of HDACs clearly emphasises that inhibition of these enzymes would be clinically significant and might open new therapeutic routes.

HDAC inhibitors have now been extensively investigated for treatment against cancer and other human pathologies. Suberoylanilide hydroxamic acid (SAHA), a hydroxamic acid derivative, is used for treating cutaneous T-cell lymphoma. Recently, Romidepsin has gained FDA approval for treating cutaneous and peripheral T-cell lymphoma (Ververis, Hiong, Karagiannis, & Licciardi, 2013). Benzamide derivatives like CI-994 and MS-275; cyclic tetrapeptides like apicidin, trapoxin, HC-toxin; electrophilic ketones like trifluoromethyl ketone and short chain fatty acids like valproate, sodium butyrate and phenyl butyrate have been developed as effective HDAC inhibitors (Bolden, Peart, & Johnstone, 2006).

Pharmacophore models derived for HDAC inhibitors show three distinct features: – (a) a capping group interacting with residues at the entry point of the active site; (b) a zinc-binding group (ZBG) that chelates the zinc ion at the active site making the enzyme catalytically inactive; and (c) a linker group that interacts with the hydrophobic groove of the active site (Miller, Witter, & Belvedere, 2003). Molecular dynamics simulations on Class I HDACs with diverse HDAC inhibitors have shown that interaction of the protein surface and ligand is also vital for ligand binding. The flexibility of active site residues is an influential factor in these interactions (Wang, Helquist, Wiech, & Wiest, 2005). Strategies to enhance the selectivity towards specific HDAC isoforms include modifying the capping group, linker or the ZBG (Dowling, Gantt, Gattis, Fierke, & Christianson, 2008; Vannini et al., 2004). Pharmacophore models of some hydroxamate groups have been documented (Chen, Jiang, Zhou, Yu, & You, 2008; Noureen, Kalsoom, & Rashid, 2010; Yu, Liu, Chen, & You, 2009) and E-pharmacophore mapping of Class I HDACs has been worked out recently (Kalyaanamoorthy & Chen, 2013). Though an inhibitor with higher potency than SAHA has been developed against HDAC1 through click chemistry (Sun et al., 2013), the prediction of energy-optimised pharmacophore of Class II HDACs has not been attempted yet. The functional involvement of Class II HDACs in developmental disorders and neurodegenerative signalling reflects the need for specific inhibitors of this class. The current work attempts to identify the factors that confer isoform specificity to Class II HDAC enzymes. In this work, 18 HDACi from structurally diverse HDAC inhibitor groups with experimentally reported IC_{50} values (Bradner et al., 2010) were chosen and docked flexibly against different Class II HDAC receptors. The interactions of the HDACs with each of their HDAC inhibitors have been investigated in detail. Binding Free Energy (BFE) estimates were done using molecular mechanics-generalised born surface area (MMGBSA) approaches and an energy-optimised pharmacophore (E-pharmacophore) approach was used for predicting the pharmacophore features of diverse group of HDAC inhibitors against Class II HDACs. The features emerging from this work will be useful in designing novel, high potent and isoform-specific Class II HDAC inhibitors.

2. Materials and methods

2.1. Protein preparation

The structures of two Class II HDACs – HDAC4 and HDAC7 were considered as initial reference structures to understand the structural behaviour of HDACs 5, 6, 9 and 10. Crystal structures of HDAC4 and HDAC7 (PDB ID: 2VQM and 3C10) were retrieved from the Protein Data Bank (http://www.rcsb.org). Sequences for HDAC5 (Q9UQL6), HDAC6 (Q9UBN7), HDAC9 (Q8WUI4) and HDAC10 (Q9UKV0) were retrieved from Swiss-Prot (http://www.uniprot.org). Since the HDACs considered in the study showed a sequence identity of 76% with HDAC4, the template which possesses a crystal structure, homology modelling was employed to model the HDACs whose structures were not available. The structure of HDAC4 (PDB ID: 2VQM) was chosen as the appropriate template for modelling all the target sequences considered. The models were validated using PROCHECK for its stereochemical quality (Wu et al., 2012). Protein preparation was done using Schrödinger Suite and the bond orders and formal charges added to hetero groups. Addition of appropriate number of hydrogen atoms and generation of metal-binding sites were done to optimise the structures. Water molecules were removed from the structures. To predict the conformations of structures with missing side chains, refinement was done with the prime module of Schrödinger. A brief relaxation was performed for each structure using the OPLS-2005 forcefield to reduce steric clashes that may exist in the crystal PDB structures (Salam, Nuti, & Sherman, 2009). Grid generation for crystal structures was done with the co-crystallised ligand as the centroid, while in modelled structures the grid was generated with the zinc atom as the centroid.

2.2. Ligand preparation

The structures of ligands from diverse groups of HDACi like hydroxamic acids, benzamide derivatives, cyclic tetrapeptides and short chain fatty acids were drawn using ChemSketch. The structures were then prepared for docking using LigPrep (LigPrep) module of Schrödinger Suite. Ligands were subjected to minimisation and the ionisation states were considered in the pH range of 5–9 (active pH range for proteins). Metal-binding states of ligands were also generated apart from three low-energy ring conformations. Ligand molecules were desalted to remove the counter ions and were optimised using the OPLS-2005 Force Field.

2.3. Docking and BFE calculations

The 18 HDAC inhibitors chosen for the study were docked to their six receptors (Class II HDACs) using the module Glide (Glide) of the Schrödinger Suite and the calculations were done using the extra precision mode of Glide (Friesner et al., 2006). MMGBSA (from the Prime 3.1 module of the Schrödinger Suite) approach was used for calculating the binding free energies of the docked complexes (HDAC and the HDACi). An internal dielectric constant of 1 and an external dielectric constant of 80 (default dielectric constants) were employed. The internal dielectric constant here refers to the dielectric constant employed within the radius of an atom ($\mathcal{E}=1$) and the external dielectric constant refers to the dielectric constant of the continuum solvation model ($\mathcal{E}=80$). The MMGBSA predicts ligand binding energies and ligand strain energies for a set of ligands docked to a single receptor using the equation (Lyne, Lamb, & Saeh, 2006),

$$\Delta G_{\mathrm{b}} = \Delta E_{\mathrm{MM}} + \Delta G_{\mathrm{solv}} + \Delta G_{\mathrm{SA}}$$

where ΔE_{MM} is the difference between the minimised energies of ligand–protein complex and the total energies of protein and ligand in free form. ΔG_{solv} is the difference in the GBSA solvation energies of the HDAC-HDACi complex and the sum of the solvation energies of HDAC and HDACi in the unbound state. ΔG_{SA} is the difference in the surface area energies for the free HDAC enzymes and HDACi (Hou, Wang, Li, & Wang, 2011). The values of BFE thus obtained were then compared with the *in vitro* IC_{50} values of corresponding HDAC inhibitors used in primary human erythroid progenitor cells (Bradner et al., 2010). In order to verify the correlations in the observed IC_{50} values, MMGBSA was carried out both at (a) the frozen (or the non flexible state) where the receptor was kept fixed and no relaxation was allowed for the receptor and (b) a state where the residues in the receptor within 4 Å from the ligand were allowed to move (Kosti, Lambrinidis, Myrianthopoulos, Diallinas, & Mikros, 2012; Vilar, Karpiak, & Costanzi, 2010).

2.4. Energy-optimised structure-based pharmacophore predictions

E-pharmacophore models in general are created to identify the bioactive spots of a ligand in its least energy state. The generation of the E-pharmacophore requires the complex of the receptor and its ligand (HDAC-HDACi complex) in its least energy conformation. The energy terms are then mapped to the atom centres through a scoring function (Glide XP) involving hydrogen bond, van der Waals and hydrophobic interactions. Pharmacophoric sites with a default set of six characteristics such as hydrogen bond donors (HBDs), hydrogen bond acceptor (HBAs), hydrophobic site, aromatic ring, positive ionisable group and negative ionisable group (Salam et al., 2009; Yoo & Medina-Franco, 2011) are then generated. The sum of the energy contribution of atoms is assigned to the respective pharmacophoric feature. This mapping enables energy quantification of ligand sites within the receptor environment.

As the ligands in this study belong to four structurally different groups, one representative from each group was chosen based on the highest G- score and were subjected to e-pharmacophore analysis using single ligand approach.

3. Results and discussion

3.1. Structure validation

3D models of HDAC5, HDAC6, HDAC9 and HDAC10 obtained through homology modelling were tested for stereochemical quality using PROCHECK (Laskowski, MacArthur, Moss, & Thornton, 1993). These structures presented 99.6, 98.9, 98.8 and 99.3% for HDAC5, HDAC6, HDAC9 and HDAC10, respectively. in the allowed regions. The Verify 3D evaluation presented refined structures, which were then minimised to convergence (Lüthy, Bowie, & Eisenberg, 1992).

3.2. Structural alignment of Class II HDAC models

The homology models of the different Class II HDACs were superposed with the template structures to understand the structural identity across the isoforms. The HDACs aligned well structurally yielding a backbone rmsd of 0.5 Å between the available crystal structures (templates) and the homology models as represented in Figure 1. The sequence identity ranged between 74 and 76% for Class IIa HDACs (Supplementary Figure S1).

3.3. Molecular docking

In order to extract information on significant ligand characteristics that arise during the interactions between HDACs and their inhibitors, 18 HDACi from diverse

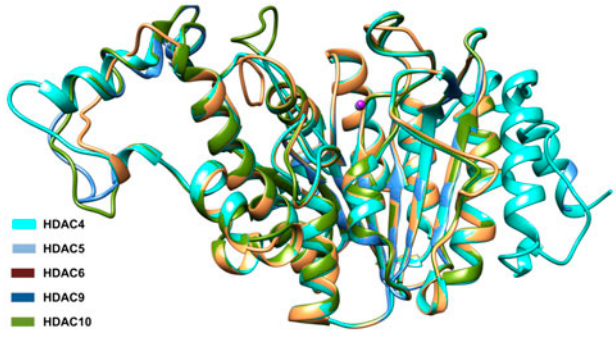

Figure 1. Structural superposition of isoforms of Class II HDACs. Here, the superposition of the backbone of HDAC4 (crystal structure) and of HDACs 5, 6, 9, 10 (homology models) have been shown for clarity. The zinc cation is represented as purple sphere. The rmsd of the HDAC structures is 0.5 Å.

structural groups were docked against each of the members of the Class II HDAC family. The inhibitors whose *in vitro* IC_{50} values were determined for all the selected ligands against a single cell line under similar experimental conditions were chosen for investigation (Bradner et al., 2010). The G-scores (reflective of binding affinities) obtained from the 108 docked complexes are shown in Figure 2 and Supplementary Table ST1. The lists of HDACi chosen are diverse and are hydroxamates, benzamide derivatives, cyclic tetrapeptides and short chain fatty acids with novel and investigational applications (Supplementary Figure S2). The docking sites of NK57 on HDAC4 and that of LAQ824 on HDAC7 are shown in Figure 3(a) and (b), respectively. Most of the inhibitors discussed in this work dock to the same binding region on the Class II HDAC considered as shown in Figure 3(c). We have performed re-docking of the native ligands (bound) of 2VQM (hydroxamic acid inhibitor) and of 3C10 (Trichostatin A) and the rmsd between the native and the re-docked poses was 1.97Å and 0.97Å, respectively, for 2VQM and 3C10.

3.4. *Evaluation of G- Scores*

Of the HDAC inhibitors chosen, the inhibitor NK57 which belongs to hydroxamate group showed highest G-scores of –10.47, –8.03 and –11.27 with HDAC4, HDAC5 and HDAC6 and hence a higher affinity in docking to these HDACs. Tubacin, yet another inhibitor in the hydroxamate group showed a score of –10.87 with HDAC6 and hence may be a viable candidate in inhibiting HDAC6. Tubacin has been reported by many workers as a potent inhibitor of HDAC6 both *in silico* as well as *in vitro* supporting our *in silico* predictions (Estiu et al., 2008; Haggarty, Koeller, Wong, Grozinger, & Schreiber, 2003; Namdar, Perez, Ngo, & Marks, 2010). LAQ824, a member of the hydroxamate group, showed high G-scores of –11.87 and –11.62 with HDAC7 and HDAC9, respectively, while docking with a slightly reduced affinity with HDAC6 with a G-score of –10.65. These results align well with experimental evidences reporting LAQ824 as the potent inhibitor of HDAC6 and HDAC7 (Khan et al., 2008). The observation that Tubacin which ranked second against all inhibitors of HDAC6 proved to be the best inhibitor of HDAC10 with a G-score of –9.98 derives support from experimental findings that HDAC6 and HDAC10 share unusual structural and pharmacological characteristics (Guardiola & Yao, 2002).

Among HDAC inhibitors of the benzamide group, CI-994 proved to be the best inhibitor of HDAC4 and HDAC5 with G-scores of –8.51 and –5.37, respectively. MS-275 scored higher affinity on its interactions with

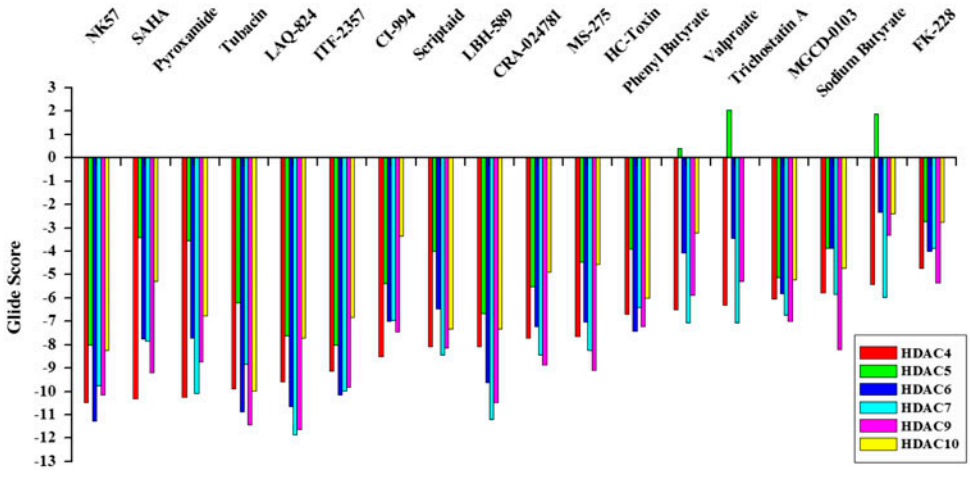

Figure 2. Glide scores of structurally diverse HDAC inhibitors against Class II HDAC isoforms.

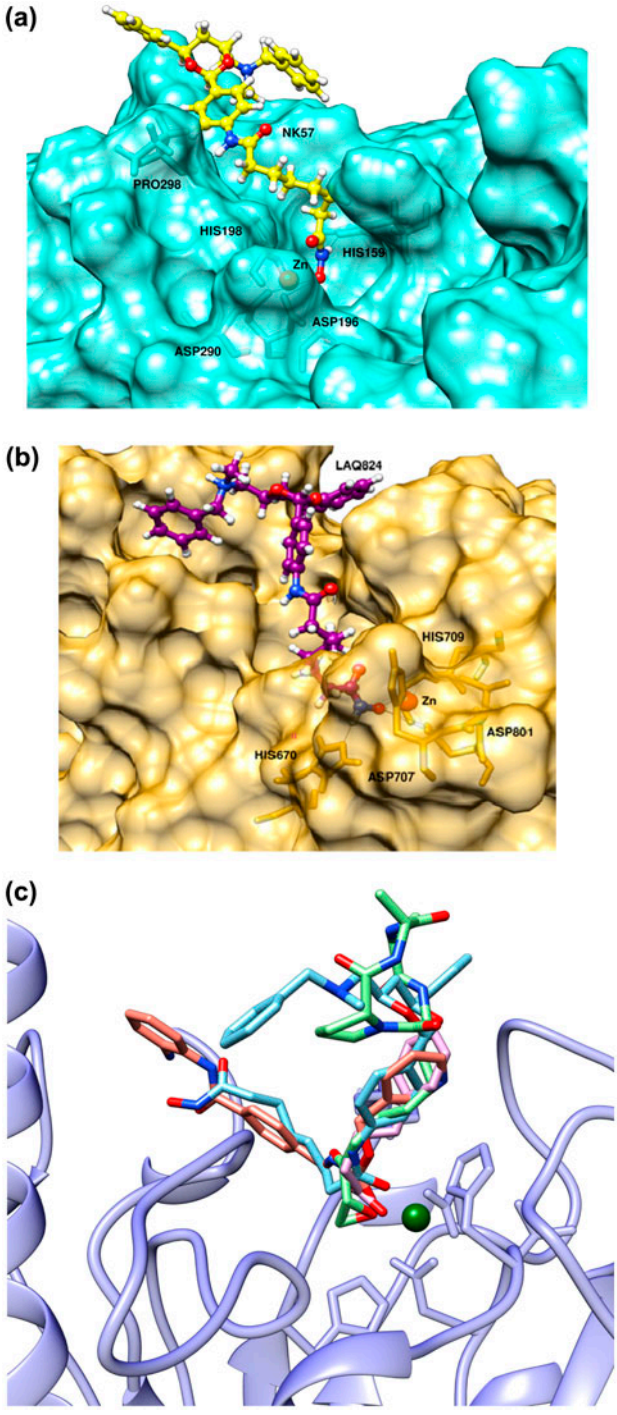

Figure 3. Complexes of HDAC4 and HDAC7 docked with HDAC inhibitors NK57 and LAQ824 respectively. The active site residues involved in charge relay mechanism by HDACi are shown in black (a) NK57 shows interactions with HIS159, ASP196 and ASP290 of HDAC4 (b) LAQ824 shows interactions with HIS670, ASP707 and ASP801 of HDAC7. Hydrogen bond interactions are represented by black solid lines (c) HDAC6 structure docked with diverse ligands demonstrates that all inhibitors target similar binding sites.

HDAC6, HDAC7, HDAC9 and HDAC10. MS-275 with G-Scores of –7.02,–8.24,–9.10 and –4.55, respectively, compared to CI-994 (Supplementary Table ST1). Our docking attempts predicted HC-toxin to be the best inhibitor of Class II HDACs and Phenyl butyrate to be the most potent inhibitor among short chain fatty acids. We hypothesise that the enhanced inhibitory potential of Phenyl butyrate as compared to Valproate and Sodium butyrate is due to presence of high-scoring aromatic ring in the Zn-binding group. A similar observation was proven valid for Class I HDACs also in a recent paper (Kalyaanamoorthy & Chen, 2013). Sodium butyrate showed weak affinity towards HDAC5 (G-score 1.87), HDAC6 (G-score –2.32) and HDAC10 (G-score –2.40). This observation is in alignment with previous reports that HDAC6 is resistant to inhibition of Trapoxin and Sodium butyrate (Hubbert et al., 2002).

Our docking efforts establish that hydroxamates like NK57, Tubacin and LAQ824 show higher affinity to various isoforms of Class II HDACs, while short chain fatty acids such as Sodium butyrate show lower affinity in inhibiting isoforms of various Class II HDACs.

3.5. Interaction profile of HDAC inhibitors with Class II HDACs

In order to obtain a better understanding of the interaction profiles of HDAC inhibitors with Class II HDACs, we chose the top scoring inhibitors from diverse groups and analysed their interactions with the Class II HDACs they were docked with. We derived ligand interaction diagrams portraying the key residues involved in the docking of the 18 HDAC inhibitors chosen against all the six Class II HDACs involved in the study and analysed the pattern of interactions of hydroxamates, cyclic tetrapeptides, benzamide derivatives and short chain fatty acids family of HDAC inhibitors individually (Representative ligand interaction diagrams are shown in Figure 4(a) and (b)).

Class IIa HDACs show strong hydrogen bonding through their histidine residues at various sites with hydroxamate groups of inhibitors like NK57 and Tubacin (Supplementary Table ST2a) besides interacting with Aspartate, Proline and Glycine in their active site.

Interestingly, while inhibiting HDAC7, the His670 of the deacetylase enzyme interacts with all inhibitors of the hydroxamate family as shown in Supplementary Table ST2b. It is also observed that Gly285 is favoured by inhibitors of the short chain fatty acid group like Valproic Acid and Phenyl butyrate, and by cyclic tetra peptides like HC-Toxin. While inhibiting HDAC9, all types of HDAC inhibitors favoured interactions with His158 of HDAC9.

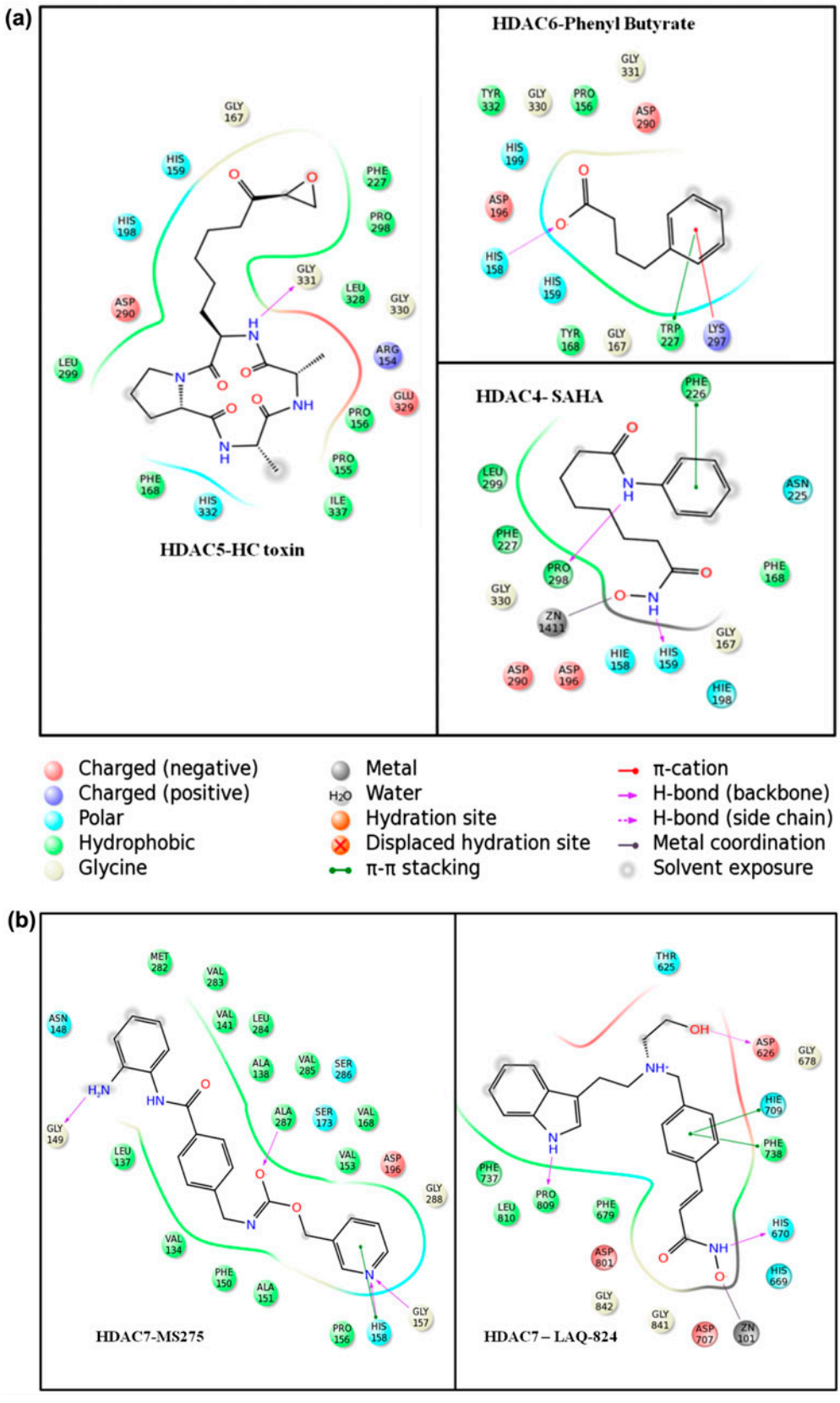

Figure 4. (a, b) Ligand interactions diagrams of Class II HDAC isoforms inhibited by HDACi. Residues within the zone of interaction of 5 Å are shown.

The Class IIb HDACs like HDAC6 show preferential hydrogen bond interactions with hydroxamate group inhibitors through Gly167 and π–π interactions through His198, Trp227 and Tyr168, while short chain fatty acids like Valproic acid and Phenyl butyrate interact through His 158 of HDAC6 and favour less π-π interactions. HDAC10 interacts with inhibitors like SAHA, HC-Toxin and Phenyl butyrate through its histidines at positions 158 or 159. Lower numbers of π-π interactions in these HDACs are mediated by phenylalanine and tyrosine (Supplementary Table ST2a).

In summary, it is observed that histidines are heavily involved in hydrogen bonding with HDAC inhibitors belonging to diverse groups and that the π-π interactions are driven by phenylalanine and histidine residues in various HDACs. The active site in most of these interactions is formed by histidine, aspartate, tyrosine, phenylalanine and tryptophan. It is possible that these residues may contribute to HDAC activity. HDACi prefer histidine and aspartate residues for hydrogen bonding in Class IIa HDACs, while preferring glycine and arginine for hydrogen bonding in case of Class IIb HDACs. Class IIa HDACs show π-π interactions with HDACi through phenylalanine and histidine residues, while same interactions are shown by histidine, tyrosine and tryptophan residues with HDACi in case of Class IIb HDACs. Comparatively, HDAC inhibitors show hydrogen bonding with His145, His146, Gly134 and Asp164 of Class I HDACs, while forming π-π interactions with histidine residues at various positions of Class I HDACs (Kalyaanamoorthy & Chen, 2013).

HDACs use charge relay mechanism like serine proteases to perform deacetylase activity. Such charge relay mechanisms requires one histidine and two aspartate residues with Zinc cation playing a pivotal role in this mechanism. Irrespective of the groups they belong to, the HDACs make charge relay system dysfunctional by chelating the Zn ion in their structures (Finnin et al., 1999). Our docking efforts showed interactions of NK57 with one histidine residue His159 and two Aspartate residues, Asp290 and Asp196, apart from the Zn ion at the active site of HDAC4. This validates a probable inhibitory mechanism prevalent in HDAC inhibitors. Similarly, LAQ824 interacts with the His670, Asp801 and Asp707 besides Zn at the active site of HDAC7 thereby impairing its charge relay mechanism. Figure 3(a) and (b) display the interacting residues in case of NK57 and LAQ824 with HDAC4 and HDAC7, respectively. Hydroxamates which make multiple hydrogen bonds and π-π interactions with active site residues of Class II HDACs provide clear evidence of why these inhibitors show high G-score and the highest binding affinity. Short chain fatty acids have shorter linker region and thus cannot access the deep-seated Zn easily. The shorter linker also makes less hydrophobic interactions with the cleft of active site. The absence or scarcity of aromatic rings in short chain fatty acids like Valproate, Sodium butyrate and Phenyl butyrate reduces their capacity of forming π-π interactions apart from interacting with active site gate residues. These features may explain the least negative G-score and weaker binding affinity of these inhibitors.

3.6. *Inhibitory potential is not Zn distance dependent*

HDAC inhibitors chelate zinc by using oxygen atom of their ZBGs. The distance between the oxygen atom and the zinc ion was measured in all the best scoring energetically favourable structures among different groups of HDACi. Both LAQ824 (most potent inhibitor against HDAC7) and Phenyl butyrate (a less potent inhibitor) showed a similar zinc distance of 1.99 Å. In the same way, in case of HDAC4, CI-994 which is more potent than Phenyl butyrate showed a zinc distance of 2.062 Å compared to the latter at a distance of 1.979 Å. Thus, the distance of zinc cation from ZBG of inhibitor is immaterial for its potency.

3.7. *Estimates of BFE*

We calculated the BFE of the 108 docked complexes MMGBSA. BFE values obtained were correlated with the known *in vitro* IC_{50} values of the respective inhibitors (Bradner et al., 2010). The lower the BFE, the more the interactions between the inhibitor and the receptor, and lesser the IC_{50} value, the higher the affinity of the inhibitor. Inhibitors with high IC_{50} values greater than 1000 µM like Sodium butyrate, Valproate and Phenyl butyrate showed least binding as evidenced by less favourable binding free energies (Figure 5 and Supplementary Table ST3). These findings are supported by the observations that inhibitors lacking aromatic ring in the linker regions are feeble inhibitors. When the HDACs were held rigid without flexibility in movement, a strong positive correlation was observed between the BFE and IC_{50} values. This is similar to observations of maximum correlation observed when β_2-adrenergic receptor was held without flexibility against agonists and antagonists (Vilar et al., 2010). Our calculations showed a high Pearson's Correlation coefficient (R) of 0.87 for HDAC7 and 0.81 for HDAC4. HDAC6 showed a correlation coefficient of 0.72, while HDAC5 and HDAC9 showed a value of 0.78 and 0.54, respectively. HDACi like NK57 and Tubacin showed higher docking affinity with the least BFE. As observed with IC_{50} values, the inhibitors possessing less G-Score like Sodium butyrate and Valproate showed low binding affinity expectedly.

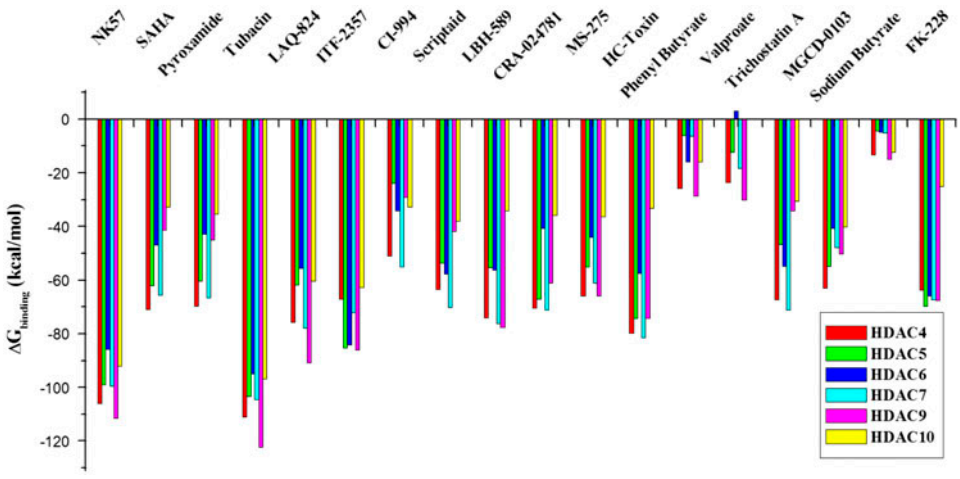

Figure 5. BFE values of structurally diverse HDAC inhibitors against Class II HDAC isoforms.

3.8. *Extracting E-pharmacophore features*

An ideal pharmacophore is an ensemble of features essential for biological activity (complementary to the receptor). To elucidate a ligand-based pharmacophore model (receptor is not considered or not known), we involve more than one ligand and generate a common featured model with these active compounds. But the energy-based model discussed in this mansucript involves docking the active compound to the binding pocket of the receptor and prioritises the features based on their binding energy. As in the case of energy-based methods, this also involves the receptor to generate complementary features; however, one active compound is sufficient to elucidate the complementary features. Hence, to explore the pharmacophore features of different HDAC inhibitors from diverse structural groups studied in the present work, we chose the highest scoring inhibitor from each group against individual Class II HDACs.

3.8.1. *E-pharmacophore features – inhibition of HDAC4*

We selected NK57, CI994, HC-toxin and Phenyl butyrate as representatives from hydroxamates, benzamide derivatives, cyclic tetrapeptides and short chain fatty acids, respectively, since they showed the highest G-Score against HDAC4 as evidenced by Supplementary Table ST1. Top views of these inhibitors docked against HDAC4 were subjected to E-pharmacophore prediction. Our pharmacophore model of NK57 showed three features namely aromatic ring in cap region and two HBDs, one in ZBG and another in the linker region. This is in agreement with previous reports which have shown one HBA and one aromatic ring apart from two hydrophobic groups as prime pharmacophore features of hydroxamates. The pharmacophore model of CI-994 also showed an aromatic ring in the ZBG apart from a HBD in the same group, while the pharmacophore for HC-toxin pharmacophore identified two main features of a HBA in ZBG and a donor in the cap group. We were able to identify one characteristic feature of a ring in the ZBG in the pharmacophore model of Phenyl butyrate (Figure 6 (a)–(d)). The presence of this ring in the ZBG appears to contribute to an enhanced G-Score as compared to that of Valproate and Sodium butyrate. This feature has been proven essential in interactions with Class I HDACs also (Kalyaanamoorthy & Chen, 2013).

3.8.2. *E-pharmacophore features – inhibition of HDAC5*

The pharmacophoric features during inhibition of HDAC5 were explored by considering the same set of four best scoring inhibitors chosen for HDAC4. The pharmacophore model of NK57 showed positive ionisable group in cap region, two HBA in ZBG and HBD in ZBG apart from two aryl rings in cap region. The features from CI-994 and HC-toxin are shown in (Figure 6(i–k)).

3.8.3. *E-pharmacophore features – inhibition of HDAC6*

To explore the pharmacophore features emerging from inhibiting HDAC6, MS-275 was selected among benzamides instead of CI-994, as it recorded the highest G-score in case of HDAC6. The other three inhibitors were retained as in earlier cases. In the case of HDAC6, NK57 exhibited five significant features: three rings in cap region, one negative ionisable group in ZBG and one HBD in linker region. MS-275 showed one ring in

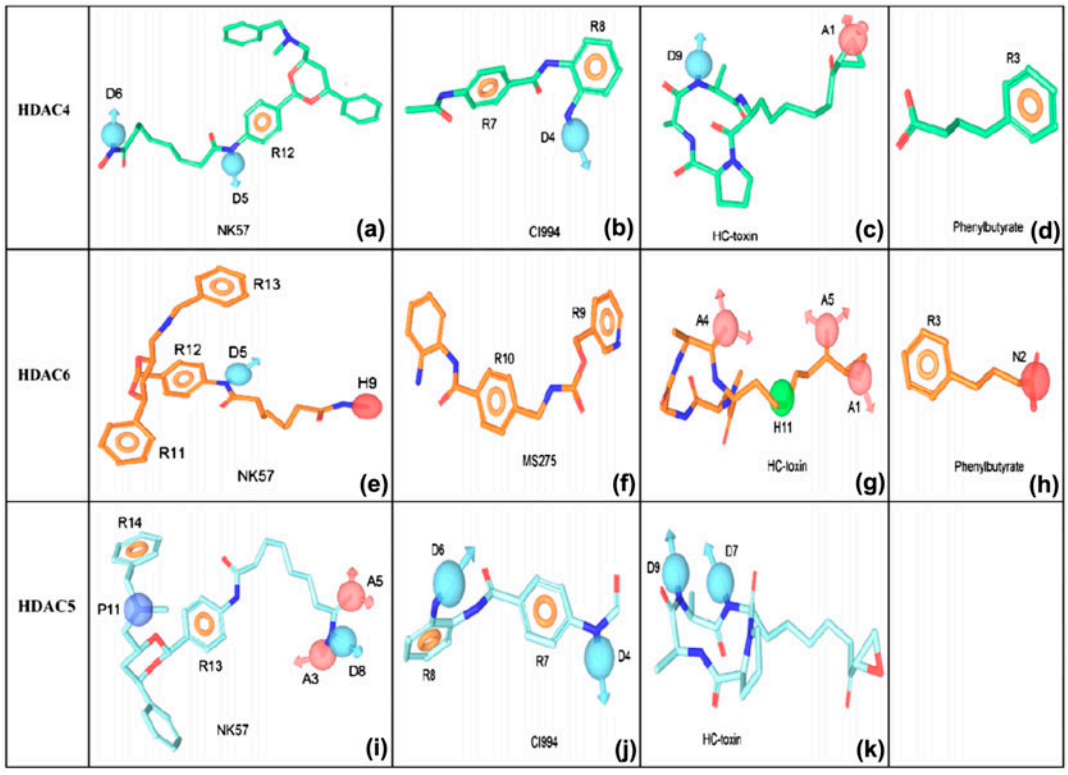

Figure 6. (a–k) Pharmacophore features of top scoring representatives of each HDAC inhibitor group against HDAC4, HDAC5 and HDAC6. "D" represents hydrogen bond donor – HBD, "A" represents hydrogen bond donor – HBA, "R" represents aromatic ring, "N" represents negative ionizable group, "P" represents positive ionisable group, "H" represents hydrophobic group.

the cap region and another in the linker region as two prominent features as against previous reports on MS 275 for Class I HDACs that the pharmacophore for MS-275 comprises three aromatic rings and one negative ionisable group apart from four HBAs and donors (Kalyaanamoorthy & Chen, 2013). HC toxin pharmacophore revealed four features in case of HDAC6 compared to HDAC4 and HDAC5 where it showed only two features. Phenyl butyrate showed two features in case of HDAC6, one being presence of ring in ZBG and another being negative ionisable group (Figure 6(e), (f), (j) and (k)).

3.8.4. *E-pharmacophore features – inhibition of HDAC7*

For predicting the pharmacophore features of best scoring inhibitors against HDAC7, we selected LAQ824 as hydroxamate representative, MS-275 as benzamide derivative representative, HC-toxin as cyclic tetra peptide representative and phenyl butyrate as short chain fatty acid group representative. Our pharmacophore model for LAQ824 showed five features, namely HBD in cap region, aromatic ring in linker region, aromatic ring in cap region and two HBDs of which one in ZBG and another in linker region. In case of Class I HDACs, two HBAs, two HBDs in ZBG and one aromatic ring in linker region are the pharmacophoric features reported earlier (Kalyaanamoorthy & Chen, 2013). The pharmacophore of HC-toxin displayed two features, one HBD in cap region and another HBA in ZBG, while Phenyl butyrate featured an aromatic ring in the ZBG (Figure 7(a)–(d) respectively).

3.8.5. *E-pharmacophore features – inhibition of HDAC9 and HDAC10*

The four inhibitors mentioned in case of HDAC7 were also selected for HDAC9 as they scored top ranks in their respective groups. Contrary to HDAC7, LAQ824 showed nine critical features in case of HDAC9. These features are three HBDs, two in ZBG and one in the cap region, and three aromatic rings, two in the cap region and one in linker apart from one acceptor in cap group. Earlier pharmacophoric features for same inhibitor against Class I HDAC HDAC8 had also predicted nine features, namely four HBAs, three HBDs and two aromatic rings (Noureen et al., 2010). In case of Class II HDACs, an extra aromatic ring is in LAQ824 compared to Class I HDACs. As regards HDAC9, three extra

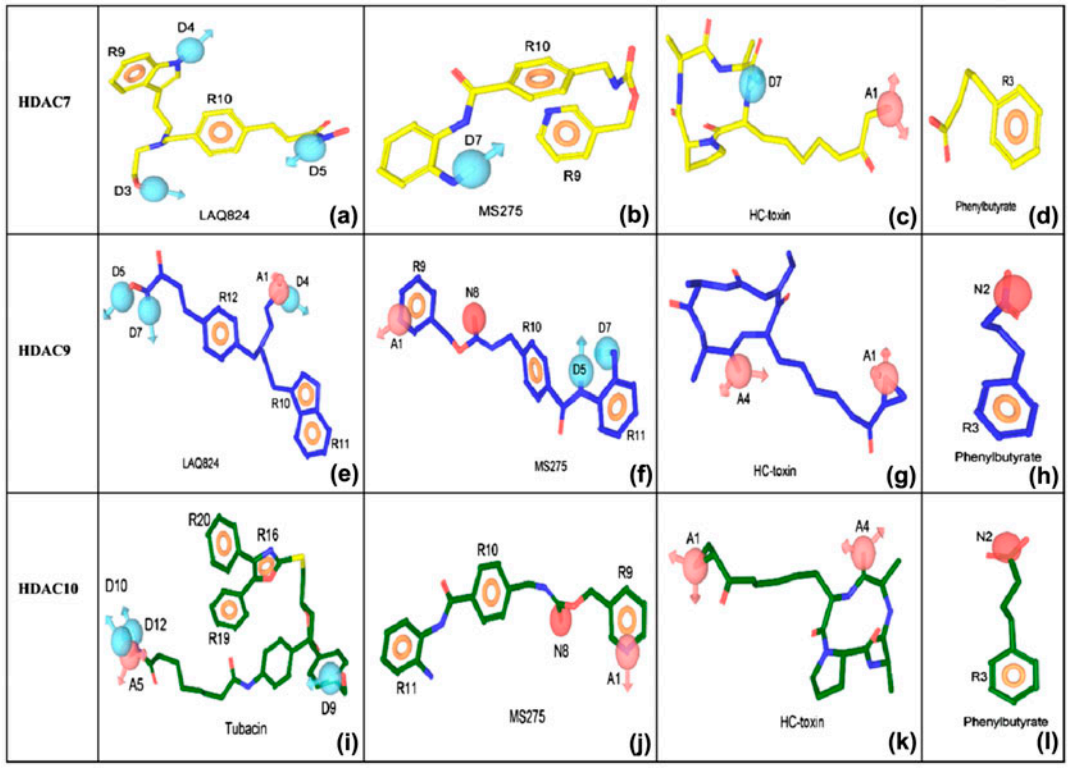

Figure 7. (a–l) Pharmacophore features of top scoring representatives of each HDAC inhibitor group against HDAC7, HDAC9 and HDAC10. Description of letters is same as in Figure 6.

HBAs are present in the predicted pharmacophoric features of the same inhibitor. Compared to HDAC7, MS-275 in case of HDAC9 showed seven important features, namely HBA in cap region, three aromatic rings one in every region of HDACi and two HBDs in ZBG. In case of Class I HDACs, 12 features have been reported for MS-275 (Kalyaanamoorthy & Chen, 2013). HC-toxin showed two HBAs – one in the cap region and another in ZBG. Compared to HDAC7, phenyl butyrate showed two features of a negative ionisable group and a ring in ZBG (Figure 7(e)–(h)).

Considering the inhibition of HDAC10, Tubacin was considered the hydroxamate representative as its G-score was the highest against HDAC10. Other three inhibitors remained same in this case also. Seven pharmacophoric features were predicted for Tubacin in case of HDAC10. These features include three aromatic rings in cap group and three HBDs, two in ZBG and another in cap group apart from one HBA in cap group. MS-275 showed three rings one in each region. In addition to these, one HBA and one negative ionisable group were also present in the cap region. Pharmocophore features of HC-toxin and Phenyl butyrate were same as in case of HDAC9 (Figure 7(i)–(l), respectively).

It can thus be observed that the pharmacophoric features generated in this work for top rank inhibitors could relate to the energy contribution of each pharmacophoric feature quantitatively. In the case of hydroxamate representatives, the ring in cap region (R_C) contributes dominantly to the energy of interaction against Class IIb HDACs (–1.24 kcal/mol for HDAC6 and –1.25 kcal/mol for HDAC10). In the case of HDAC4, HDAC5, HDAC7 and HDAC9, a HBD in linker region (D_L), positive ionisable group in cap region (P_C), HBD in cap region (D_C) and HBD in ZBG (D_Z) are the energy-contributing pharmacophoric features (–2.17, –2.42, –2.13 and –1.60 kcal/mole), respectively (Table 1) . Regarding benzamide derivatives like CI-994, the ring in linker (R_L) contributes to a maximum energy value (–1.03 kcal/mol) in case of HDAC4, while HBD in cap region (D_C) (–2.20 kcal/mol) overtakes this position in case of HDAC5. Regarding cyclic tetrapeptides like HC-toxin, HBD in cap region scores the highest in case of Class IIa HDACs like HDAC4 (–1.98), HDAC5 (–0.45) and HDAC7 (–2.11) except HDAC9, while in case of Class IIb HDACs, HBA in ZBG (A_Z) contributes maximum score in terms of energy. In case of Class I HDACs, the maximum energy-scoring feature is ring in linker in case of CI-994, MS-275 and LAQ824 (Kalyaanamoorthy & Chen, 2013). The pharmacophoric features of HDACi contributing to the energy score are shown in detail in Table 1.

Table 1. E-pharmacophore scores of top ranking HDAC inhibitor.

HDAC inhibitor	HDAC4	HDAC5	HDAC6	HDAC inhibitor	HDAC7	HDAC9	HDAC10
NK57				LAQ-824		D_Z: –1.60	
		P_C: −2.42	R_C: –1.42		D_C: −2.13	R_L: −1.08	
	D_L: −2.17	A_Z: −1.60	N_Z: −0.90		R_L: −1.47	R_C: –0.81	
	D_Z: −0.64	R_C: −1.34	D_L: –0.70		D_Z: −0.59	R_C: −0.57	
	R_C: −0.82	R_C: −0.79	R_C: −0.68		R_C : –0.51	D_C: −0.55	
		D_Z: −0.63	R_C : –0.48		D_L: −0.31	D_Z: −0.51	
		A_Z: −0.59				A_C: −0.50	
Tubacin							R_C : –1.25
							D_Z: −1.04
							A_Z : –0.80
							R_C: −0.80
							D_C: −0.66
							D_Z: −0.30
							A_Z: −0.35
							A_C: −0.28
			A_Z: −0.66				
HC-Toxin	D_C: −1.98	D_C: –0.45	A_C: −0.66		D_C: −2.11	A_Z: −1.04	A_Z: −0.35
	A_Z: −0.67	D_C: −0.02	H_L: −0.19		A_Z : −0.67	A_C: −0.32	A_C: −0.28
			A_Z: −0.17				
CI-994		D_C: −2.20					
	R_L: −1.03	R_L: −1.21					
	R_Z: −0.74	R_Z: −0.78					
	D_Z : –0.66	D_Z: −0.25					
MS-275						A_C: −2.17	R_C: −1.39
						R_C: −0.99	A_C: −0.70
			R_L: −1.39		R_C: −1.45	R_L: −0.77	N_C: −0.35
			R_C: −1.07		R_L: −1.41	R_Z: −0.69	R_Z: −0.95
					D_Z: −0.17	D_Z: −0.66	R_C: −0.75
						N_C: −0.32	
phenyl butyrate	R_Z: −1.26		R_Z: −0.94		R_Z: −1.72	N_Z: −1.03	R_Z: −1.23
			N_Z: −0.62			R_Z: −0.74	N_Z: −0.90

Note: The high scoring pharmacophoric features of top ranking HDACi against every member of Class II HDAC are given. Here D_L, D_C and D_Z represents HBD in linker region, cap region and ZBG respectively. A_L, A_C, A_Z represent HBA in linker, cap and ZBG. P_C and N_C represent positive and negative ionizable group in cap region respectively. R_L, R_C, R_Z represent ring in linker, cap and ZBG respectively. H_L signifies hydrophobic group in linker region. N_Z represents negative ionizable group in ZBG.

Conclusions

In this work, we have employed a combinatorial approach using *in silico* docking and E-pharmacophore mapping to understand the significances of structural variations during interactions of HDACis with a variety of Class II HDACs. Towards this, we evaluated the interacting mechanisms of structurally diverse HDAC inhibitors of hydroxamates, benzamides, cyclic tetrapeptides and short chain fatty acids against Class II HDACs through rigorous docking. The HDAC interaction profiles show a significant involvement of histidines and aspartates in the hydrogen bonding between the diverse HDAC inhibitors explored in the work. It was also observed that π-π interactions are driven by phenylalanine, histidine, tryptophan and tyrosine residues in various HDACs. Previous studies on Class I HDACs have shown that HDAC inhibitors prefer hydrogen bonding with His145, His146, Gly134 and Asp164 of Class I HDACs, while forming π-π interactions with histidine residues at various positions of Class I HDACs (Kalyaanamoorthy & Chen, 2013).

Charge relay mechanisms in HDACs require one histidine and two aspartate residues with a zinc cation. It is known that the charge relay system is rendered dysfunctional by HDACs through chelation of the zinc ion in the HDAC structure (Finnin et al., 1999). Our docking efforts showed interactions of NK57 with one histidine residue (His159) and two aspartate residues (Asp290 and Asp196) apart from the zinc ion at the active site of HDAC4 pointing to a valid inhibitory mechanism typical of HDAC inhibitors.

A strong positive correlation was observed between the estimated BFE of these complexes and the experimentally derived IC_{50} values of HDAC inhibitors (Bradner et al., 2010). Besides a validated accuracy of the MMGBSA calculations attempted here, the interaction profile and energy values present interesting observations and connections between the inhibitory potential of HDACi and the structures of HDACs which they inhibit. Our sets of computational experiments establish hydroxamate-based HDACi as being effective inhibitors of Class II HDACs. It is observed that

inhibitors NK57 and Tubacin which show more potency against HDAC4, HDAC5, HDAC6 and HDAC10 show the maximum number of rings (four and six) in their cap region. LAQ824, which shows highest potential to inhibit HDAC7 and HDAC9, possesses aromatic rings in both its cap and linker regions.

Benzamide derivative types of HDAC inhibitors show a structure-dependent interaction profile different from that of their hydroxamate counterparts. The inhibitor CI-994 which shows the highest inhibitory potential against HDAC4 and HDAC5 contains aryl rings in ZBG and the linker region. This validates the requirement that a benzamide derivative to be the most potent for HDAC6, HDAC7, HDAC9 and HDAC10 should possess aryl rings at all the three vital regions as in MS-275.

Our investigations show that cyclic tetrapeptides such as HC-toxin with higher inhibitory potential have long linker regions, while the presence of an aromatic ring in the ZBG enhances potency among short chain fatty acid-based inhibitors.

LAQ824 shows an extra aromatic ring as an important feature in case of Class II HDACs compared to Class I. These features can be utilised for virtual screening of specific inhibitors. This aids us to hypothesise that the presence of aromatic rings in the HDACi structure enhances its potency to inhibit irrespective of the group to which it belongs.

Our attempts to quantify energies supplemented by E-pharmacophore mapping reveal that structurally different HDAC inhibitors may or may not share the same pharmacophoric features with maximum energy functionally or positionally. In a recent work, the potency of inhibitors of Class I HDACs has been correlated to the presence of aromatic rings in the linker region (Kalyaanamoorthy & Chen, 2013). Our findings on Class II HDACs show that the maximum scoring features of pharmacophore need not be attributed to the number or position of aromatic rings only but also to the presence of positive ionisable groups or HBDs in cap regions. We also observed that potent aromatic rings can be present either in the cap or the linker regions of the HDAC inhibitors. Our pharmacophore analysis leads to an interesting observation that a specific HDAC inhibitor shows different pharmacophoric features for different Class II HDACs. For e.g. LAQ824, a hydroxamate group inhibitor of HDACs, shows three HBDs and two aromatic rings in its pharmacophore for HDAC7, while incorporating three HBDs, three aromatic rings and one HBA for HDAC9. Similarly, NK57, another potent inhibitor of the same group, shows three aromatic rings, one negatively ionisable group and one HBD during its inhibition of HDAC6, while encompassing two HBDs and one aromatic ring in it pharmacophore for HDAC4, and two aromatic rings, two HBAs and one HBD apart from one positive ionisable group for HDAC5. Such observed differences in pharmacophore features can be employed for virtual screening to identify potent inhibitors against a specific isoform of Class II HDACs. In summary, the findings in this work would lead to the design of structurally variable and novel inhibitors with improved potency and desired specificity against Class II HDACs.

Supplementary material

The supplementary material for this paper is available online at http://dx.doi.10.1080/07391102.2013.879073.

Acknowledgements

The authors thank the SASTRA University for infrastructure support.

Funding

Financial support from the Department of AYUSH [Z.15015/1/2010-COE], Government of India, for the procurement of the Schrödinger Suite is gratefully acknowledged.

References

Bolden, J. E., Peart, M. J., & Johnstone, R. W. (2006). Anticancer activities of histone deacetylase inhibitors. *Nature Reviews Drug Discovery, 5*, 769–784.

Bradner, J. E., Mak, R., Tanguturi, S. K., Mazitschek, R., Haggarty, S. J., Ross, K., … Ebert, B. L. (2010). Chemical genetic strategy identifies histone deacetylase 1 (HDAC1) and HDAC2 as therapeutic targets in sickle cell disease. *Proceedings of the National Academy of Sciences, 107*, 12617–12622.

Chen, Y. D., Jiang, Y. J., Zhou, J. W., Yu, Q. S., & You, Q. D. (2008). Identification of ligand features essential for HDACs inhibitors by pharmacophore modeling. *Journal of Molecular Graphics and Modelling, 26*, 1160–1168.

Colussi, C., Mozzetta, C., Gurtner, A., Illi, B., Rosati, J., Straino, S., … Gaetano, C. (2008). HDAC2 blockade by nitric oxide and histone deacetylase inhibitors reveals a common target in Duchenne muscular dystrophy treatment. *Proceedings of the National Academy of Sciences, 105*, 19183–19187.

Van Damme, M., Crompot, E., Meuleman, N., Mineur, P., Bron, D., Lagneaux, L., & Stamatopoulos, B. (2012). HDAC isoenzyme expression is deregulated in chronic lymphocytic leukemia B-cells and has a complex prognostic significance. *Epigenetics, 7*, 1403–1412.

Dowling, D. P., Gantt, S. L., Gattis, S. G., Fierke, C. A., & Christianson, D. W. (2008). Structural studies of human histone deacetylase 8 and its site-specific variants complexed with substrate and inhibitors. *Biochemistry, 47*, 13554–13563.

Estiu, G., Greenberg, E., Harrison, C. B., Kwiatkowski, N. P., Mazitschek, R., Bradner, J. E., & Wiest, O. (2008). Structural origin of selectivity in Class II-selective histone deacetylase inhibitors. *Journal of Medicinal Chemistry, 51*, 2898–2906.

Finnin, M. S., Donigian, J. R., Cohen, A., Richon, V. M., Rifkind, R. A., Marks, P. A., ... Pavletich, N. P. (1999). Structures of a histone deacetylase homologue bound to the TSA and SAHA inhibitors. *Nature, 401*, 188–193.

Fischle, W., Kiermer, V., Dequiedt, F., & Verdin, E. (2001). The emerging role of Class II histone deacetylases. *Biochemistry and Cell Biology, 79*, 337–348.

Friesner, R. A., Murphy, R. B., Repasky, M. P., Frye, L. L., Greenwood, J. R., Halgren, T. A., ... Mainz, D. T. (2006). Extra precision glide: Docking and scoring incorporating a model of hydrophobic enclosure for protein−ligand complexes. *Journal of Medicinal Chemistry, 49*, 6177–6196.

Geng, L., Cuneo, K. C., Fu, A., Tu, T., Atadja, P. W., & Hallahan, D. E. (2006). Histone deacetylase (HDAC) inhibitor LBH589 increases duration of gamma-H2AX Foci and confines HDAC4 to the cytoplasm in irradiated non-small cell lung cancer. *Cancer Research, 66*, 11298–11304.

Glide, v. [Schrödinger]. New York, NY:LLC, 2012

Gregoretti, I. V., Lee, Y. M., & Goodson, H. V. (2004). Molecular evolution of the histone deacetylase family: Functional implications of phylogenetic analysis. *Journal of Molecular Biology, 338*, 17–31.

Guardiola, A. R., & Yao, T. P. (2002). Molecular cloning and characterization of a novel histone deacetylase HDAC10. *Journal of Biological Chemistry, 277*, 3350–3356.

Haggarty, S. J., Koeller, K. M., Wong, J. C., Grozinger, C. M., & Schreiber, S. L. (2003). Domain-selective small-molecule inhibitor of histone deacetylase 6 (HDAC6)-mediated tubulin deacetylation. *Proceedings of the National Academy of Sciences, 100*, 4389–4394.

Hou, T., Wang, J., Li, Y., & Wang, W. (2011). Assessing the performance of the MM/PBSA and MM/GBSA methods. 1. The accuracy of binding free energy calculations based on molecular dynamics simulations. *Journal of Chemical Information and Modeling, 51*, 69–82.

Hubbert, C., Guardiola, A., Shao, R., Kawaguchi, Y., Ito, A., Nixon, A., ... Yao, T. P. (2002). HDAC6 is a microtubule-associated deacetylase. *Nature, 417*, 455–458.

Kalyaanamoorthy, S., & Chen, Y. P. P. (2013). Energy based pharmacophore mapping of HDAC inhibitors against Class I HDAC enzymes. *Biochemica and Biophysica Acta, 1834*, 317–328.

Khan, N., Jeffers, M., Kumar, S., Hackett, C., Boldog, F., Khramtsov, N., … Sehested, M. (2008). Determination of the class and isoform selectivity of small-molecule histone deacetylase inhibitors. *Biochemical Journal, 409*, 581–589.

Kosti, V., Lambrinidis, G., Myrianthopoulos, V., Diallinas, G., & Mikros, E. (2012). Identification of the substrate recognition and transport pathway in a eukaryotic member of the nucleobase-ascorbate transporter (NAT) family. *PLoS One, 7*, e41939.

Kouzarides, T. (2007). Chromatin modifications and their function. *Cell, 128*, 693–705.

Kuo, M. H., & Allis, C. D. (1998). Roles of histone acetyltransferases and deacetylases in gene regulation. *Bioessays, 20*, 615–626.

Kurdistani, S. K., & Grunstein, M. (2003). Histone acetylation and deacetylation in yeast. *Nature Reviews Molecular Cell Biology, 4*, 276–284.

Laskowski, R. A., MacArthur, M. W., Moss, D. S., & Thornton, J. M. (1993). PROCHECK: A program to check the stereochemical quality of protein structures. *Journal of Applied Crystallography, 26*, 283–291.

Li, B., Carey, M., & Workman, J. L. (2007). The role of chromatin during transcription. *Cell, 128*, 707–719.

LigPrep, v.. [*Schrödinger*] New York, NY: LLC, 2012.

Lüthy, R., Bowie, J. U., & Eisenberg, D. (1992). Assessment of protein models with three-dimensional profiles. *Nature, 356*, 83–85.

Lyne, P. D., Lamb, M. L., & Saeh, J. C. (2006). Accurate prediction of the relative potencies of members of a series of kinase inhibitors using molecular docking and MM-GBSA scoring. *Journal of Medicinal Chemistry, 49*, 4805–4808.

Miller, T. A., Witter, D. J., & Belvedere, S. (2003). Histone deacetylase inhibitors. *Journal of Medicinal Chemistry, 46*, 5097–5116.

Namdar, M., Perez, G., Ngo, L., & Marks, P. A. (2010). Selective inhibition of histone deacetylase 6 (HDAC6) induces DNA damage and sensitizes transformed cells to anticancer agents. *Proceedings of the National Academy of Sciences, 107*, 20003–20008.

Noureen, N., Kalsoom, S., & Rashid, H. (2010). Ligand based pharmacophore modelling of anticancer histone deacetylase inhibitors. *African Journal of Biotechnology, 9*, 3923–3931.

Rivieccio, M. A., Brochier, C., Willis, D. E., Walker, B. A., D'Annibale, M. A., McLaughlin, K., … Langley, B. (2009). HDAC6 is a target for protection and regeneration following injury in the nervous system. *Proceedings of the National Academy of Sciences, 106*, 19599–19604.

de Ruijter, A. J., van Gennip, A. H., Caron, H. N., Kemp, S., & van van Kuilenburg, A. B. (2003). Histone deacetylases (HDACs): Characterization of the classical HDAC family. *Biochemical Journal, 370*, 737–749.

Sakuma, T., Uzawa, K., Onda, T., Shiiba, M., Yokoe, H., Shibahara, T., & Tanzawa, H. (2006). Aberrant expression of histone deacetylase 6 in oral squamous cell carcinoma. *International Journal of Oncology, 29*, 117–124.

Salam, N. K., Nuti, R., & Sherman, W. (2009). Novel method for generating structure-based pharmacophores using energetic analysis. *Journal of Cheminformatics and Modelling, 49*, 2356–2368.

Shan, B., Yao, T. P., Nguyen, H. T., Zhuo, Y., Levy, D. R., Klingsberg, R. C., ... Lasky, J. A. (2008). Requirement of HDAC6 for transforming growth Factor-1-induced epithelial-mesenchymal transition. *Journal of Biological Chemistry, 283*, 21065–21073.

Sun, Q., Yao, Y., Liu, C., Li, H., Yao, H., Xue, X., ... Jiang, S. (2013). Design, synthesis, and biological evaluation of novel histone deacetylase 1 inhibitors through click chemistry. *Bioorganic & Medicinal Chemistry Letters, 23*, 3295–3299.

Tan, J., Cang, S., Ma, Y., Petrillo, R. L., & Liu, D. (2010). Novel histone deacetylase inhibitors in clinical trials as anti-cancer agents. *Journal of Hematology & Oncology, 3*, 5.

Vannini, A., Volpari, C., Filocamo, G., Casavola, E. C., Brunetti, M., Renzoni, D., … Di Marco, S. (2004). Crystal structure of a eukaryotic zinc-dependent histone deacetylase, human HDAC8, complexed with a hydroxamic acid inhibitor. *Proceedings of the National Academy of Sciences, 101*, 15064–15069.

Ververis, K., Hiong, A., Karagiannis, T. C., & Licciardi, P. V. (2013). Histone deacetylase inhibitors (HDACIs): Multitargeted anticancer agents. *Biologics, 7*, 47–60.

Vilar, S., Karpiak, J., & Costanzi, S. (2010). Ligand and structure-based models for the prediction of ligand-receptor affinities and virtual screenings: Development and application to the β2-adrenergic receptor. *Journal of Computational Chemistry, 31*, 707–720.

Wang, D. F., Helquist, P., Wiech, N. L., & Wiest, O. (2005). Toward Selective histone deacetylase inhibitor

design: Homology modeling, docking studies, and molecular dynamics simulations of human Class I histone deacetylases. *Journal of Medicinal Chemistry, 48*, 6936–6947.

Watamoto, K., Towatari, M., Ozawa, Y., Miyata, Y., Okamoto, M., Abe, A., ... Saito, H. (2003). Altered interaction of HDAC5 with GATA-1 during MEL cell differentiation. *Oncogene, 22*, 9176–9184.

Witt, O., Deubzer, H. E., Milde, T., & Oehme, I. (2009). HDAC family: What are the cancer relevant targets? *Cancer Letters, 277*, 8–21.

Wu, D., Huang, Q., Zhang, Y., Zhang, Q., Liu, Q., Gao, J., ... Zhu, R. (2012). Screening of selective histone deacetylase inhibitors by proteochemometric modeling. *BMC Bioinformatics, 13*, 212.

Yoo, J., & Medina-Franco, J. L. (2011). Homology modeling, docking and structure-based pharmacophore of inhibitors of DNA methyltransferase. *Journal of Computer-Aided Molecular Design, 25*, 555–567.

Yu, L., Liu, F., Chen, Y., & You, Q. (2009). Pharmacophore identification of hydroxamate HDAC 1 inhibitors. *Chinese Journal of Chemistry, 27*, 557–564.